

Microhardness and optical property of chalcogenide glasses and glass-ceramics of the Sn–Sb–Se ternary system

Xuning Xue, Feifei Chen, Changgui Lin, Ruiqiang Lin, Xiaoyu Zhang, Shixun Dai, Xianghua Zhang, Wei Ji

▶ **To cite this version:**

Xuning Xue, Feifei Chen, Changgui Lin, Ruiqiang Lin, Xiaoyu Zhang, et al.. Microhardness and optical property of chalcogenide glasses and glass-ceramics of the Sn–Sb–Se ternary system. Journal of the American Ceramic Society, 2019, 10.1111/jace.15980 . hal-01952379

HAL Id: hal-01952379

https://univ-rennes.hal.science/hal-01952379

Submitted on 12 Dec 2018

HAL is a multi-disciplinary open access archive for the deposit and dissemination of scientific research documents, whether they are published or not. The documents may come from teaching and research institutions in France or abroad, or from public or private research centers.

L'archive ouverte pluridisciplinaire **HAL**, est destinée au dépôt et à la diffusion de documents scientifiques de niveau recherche, publiés ou non, émanant des établissements d'enseignement et de recherche français ou étrangers, des laboratoires publics ou privés.

Accepted Article

MR. XUNING XUE (Orcid ID : 0000-0002-7147-9763)

DR CHANGGUI LIN (Orcid ID : 0000-0002-0574-6296)

Article type : Article

Microhardness and Optical Property of Chalcogenide Glasses and Glass–Ceramics of the Sn-Sb-Se Ternary System

Xuning Xue[1, 2] | Feifei Chen[1, 2*] | Changgui Lin[1, 2] | Ruiqiang Lin[1, 2] | Xiaoyu Zhang[1, 2] | Shixun Dai[1, 2] | Xianghua Zhang[3] | Wei Ji[4]

[1]Laboratory of Infrared Materials and Devices, The Research Institute of Advanced Technologies, Ningbo University, Ningbo 315211, China

[2]Key Laboratory of Photoelectric Detection Materials and Devices of Zhejiang Province, Ningbo University, Ningbo, 315211, China

[3]Laboratory of Glasses and Ceramics, UMR 6226 CNRS-University of Rennes 1, Rennes Cedex 135042, France

[4]Department of Physics, National University of Singapore, 2 Science Drive 3, 117551, Singapore

Accepted Article

Abstract

The microhardness of chalcogenide glasses (ChGs) of the Sn-Sb-Se (SSS) ternary system was investigated, and the correlation of microhardness with the mean coordination number of the SSS ChGs was determined. To prepare infrared-transparent SSS glass–ceramics (GCs), two SSS ChGs (A, $Sn_{6.23}Sb_{14.11}Se_{79.66}$; B, $Sn_{9.8}Sb_{17.22}Se_{72.98}$; by molar composition) were selected and thermally treated at 433 and 448 K, respectively. The improved microhardness (with values that increased by 11.5 % and 7.3 % for SSS ChG A and B, respectively) of the resulting SSS GCs is attributed to the formation of Sb_2Se_3 nanocrystals.

* Author to whom correspondence should be addressed. e-mail: chenfeifei1@nbu.edu.cn.

1 | INTRODUCTION

Chalcogenide glasses (ChGs) are amorphous semiconductors[1-3] with exceptional infrared transmittance, low phonon energy, high refractive index, and large third-order optical nonlinearity with ultrafast response time. The combination of these superior optical properties has led to the consideration of ChGs as candidate photonic devices that are more promising than oxide and fluoride glasses, especially in the fields of infrared laser sources, infrared sensors and all-optical communication systems. [4-7]

However, ChGs have a layered structure composed of weak covalent bonds among dibasic chalcogen elements. [8] The weak Van der Waals' force between layers leads to the relatively poorer mechanical property and thermal stability of ChGs than those of oxide

.

Accepted Article

glasses, thereby limiting the applications of ChGs. [9] The mechanical property of ChGs can be improved by incorporating group IV and V metallic elements[10, 11] with high coordination number to cross-link the network structure of ChGs. However, the detailed relationship between the mechanical property (especially microhardness) and the cross-linking degree of the ChG network, which can be quantified using a fundamental metric called mean coordination number (MCN), has rarely been reported.[12,13] The crystallization of ChGs through laser and thermal treatment is reportedly an effective method of enhancing their microhardness.[14-18] Nanocrystal formation can been used to functionally tailor the mechanical and optical properties of ChG composites while retaining their infrared-transmittance property. [19-21]

In the present work, the microhardness of Sn-Sb-Se (SSS) ChGs, which have recently been found to exhibit superior optical and thermal properties,[22-24] was investigated. The correlation of microhardness with the MCN of SSS ChGs was also discussed through the constraint theory. By using a one-step thermal treatment process, SSS glass–ceramics (GCs) embedded with Sb_2Se_3 crystals were prepared, and the dependence of microhardness, optical, structural properties on the crystal formation was studied.

.

Accepted Article

2 | EXPERIMENTAL PROCEDURE

SSS ChGs were synthesized using high-purity polycrystalline forms of tin (5N), antimony (5N), and selenium (5N). The raw materials were weighed according to the glass composition and mixed in a precleaned quartz ampoule, which was then preheated at 373 K for 1 h to remove surface moisture. The ampoule was sealed in a vacuum, placed in a rocking furnace, and melted at 1073 K for 12 h. The melt was quenched in ice water to form bulk glass. The glass sample was then annealed at 10 K below the glass-transition temperature (T_g) for 6 h to minimize internal tension and slowly cooled to room temperature. The precise chemical composition of SSS ChGs was determined by energy-dispersive spectrometry (EDS) and listed in Table 1.

One group of SSS ChGs with a molar composition of $Sn_{6.23}Sb_{14.11}Se_{79.66}$ were thermally treated at 433 K for 2, 3, 4, 5, 6, and 8 h (series A; labeled as A-SSS-2, 3, 4, 5, 6, and 8, respectively). Another group of SSS ChGs with a molar composition of $Sn_{9.8}Sb_{17.22}Se_{72.98}$ was thermally treated at 448 K for 2, 4, 6, 8, and 10 h (series B; labeled as B-SSS-2, 4, 6, 8, and 10, respectively). All glass and GC samples were polished to mirror smoothness on both sides and to a thickness of 1 mm for subsequent optical testing.

The Vickers hardness (HV) of the samples was measured using a microhardness meter (MH-3, Everone) with a charge of 25 g for 5 s. Each sample was tested 10 times, and results were averaged. X-ray diffraction (XRD) patterns were obtained with a Bruker AXS D2

.

Accepted Article

PHASER diffractometer (voltage = 30 kV; current = 10 mA; CuKα radiation), and the step width was 0.02°. To observe crystallization in the GC samples, a scanning electron microscopy (SEM) system (Tescan VEGA3 SB-Easyprobe) was used. The absorption spectra of the samples were recorded within the range of 600–2500 nm using a UV-VIS-NIR spectrophotometer (Lamda 950, Perkin–Elmer). Fourier transform infrared (FTIR) transmission spectra in the range of 2.5–25 μm were obtained with an FTIR spectrometer (Nicolet 381). To obtain detailed information with respect to the variation of glass structure after thermal treatment, Raman spectra of the samples were obtained with a Renishaw Invia Raman laser confocal Raman spectrometer at 785 nm excitation wavelength. All of the above-mentioned tests were conducted at room temperature.

3 | RESULTS

3.1 | Microhardness of SSS ChGs.

The mechanical property of ChGs was investigated in terms of microhardness (HV), and the relationship between HV and MCN (related to the chemical order of the ChG network) was studied. To accurately calculate MCN, the chemical compositions of the SSS ChGs were determined by EDS, and MCN was estimated with the following formula:

$$\mathrm{MCN} = \frac{4x + 3y + 2z}{x + y + z} \tag{1}$$

where x, y, and z are the molar percentages of Sn, Sb, and Se, respectively. Considering that all SSS ChGs in this study were in a Se-rich state, the coordination numbers of Sn, Sb, and Se

.

Accepted Article

are assumed to be 4, 3, and 2,[23] respectively, and the calculated MCN of the SSS ChGs are given in Table 1. Fig. 1 shows a plot of HV as a function of MCN of the SSS ChGs. The plot indicates that HV presents an obvious nonlinear growth trend with increased MCN. Fig. 2 shows a plot of the Sn and Sb contents of SSS ChGs versus HV. The change trend of HV against various metal elements differed, i.e., scattered distribution occurred with Sn addition, but the trend was a general increase for Sb addition. This finding indicated that the cross-linking units constructed by the three-coordinated Sb atoms contributed more to the compactness of SSS ChGs than those constructed by the four-coordinated Sn atoms. However, to some extent, the variation in HV with Sn/Sb content (Fig. 2) is highly irregular compared with the MCN value (Fig. 1), which suggests that elemental composition does not affect hardness and that topology is the dominant influencing factor.

3.2 | Characterization of crystallinity in SSS GCs.

The XRD patterns of the SSS GCs (series A and B) are shown in Fig. 3. With prolonged thermal treatment, the appearance and growth of diffraction peaks identified as Sb_2Se_3 orthorhombic crystalline (JCPDF No. 75-1462) were observed in both series. The presence of Sb_2Se_3 crystals in the SSS GCs well agreed with the experimental results obtained in Kumar's work, [16] which demonstrates that Sn combined with Se serves as the glass former for SSS ChGs, and that Sb_2Se_3-phase crystallization is a priority over $SnSe_2$-phase crystallization.

.

Accepted Article

To directly observe crystallization in the GC samples and examine the variation in thermally treated grains, SEM images of the SSS ChG and GC samples from series B were obtained and are shown in Fig. 4. As shown in the SEM image in Fig. 4(a), the precursor glass is homogeneous and contains no notable crystal grains. After thermal treatment, raindrop-shaped Sb_2Se_3 crystals 150×500 nm^2 in size appeared in the 2 h-treated GC sample (B-SSS-2), as shown in Fig. 4(b). Interestingly the crystals grew only in number with prolonged treatment, as shown in Figs. 4(c)-4(e). When treatment duration reached 10 h, the GC sample (B-SSS-10) became highly crystallized, and the grains aggregated to form lumps >2 μm in size (Fig. 4(f)). Similar experimental results were observed in the SEM images of series A.

3.3 | Microhardness of SSS GCs.

Previous work on selenide GCs (mainly based on the Ge-Se system) have shown that GC hardness can be reduced as a result of loose structural rigidity after crystallization.[25] For the present SSS GCs, their HV values in two series as a function of treatment duration are shown in Fig. 5. The microhardness of the SSS GCs was apparently enhanced after thermal treatment, and HV linearly increased with prolonged treatment. Compared with inherent cross-linking units such as pyramidal $SbSe_3$ and tetrahedral $SnSe_4$, the Sb_2Se_3 crystals embedded in the SSS glass matrix can be considered as larger and more stable ones that significantly contributed to the overall compactness of the SSS network and consequently improved the microhardness. However, the GC samples at the end of each series (A-SSS-10

.

Accepted Article

and B-SSS-8) had HV values that were even lower than those of the precursor glasses. This finding indicated that the agglomeration of Sb_2Se_3 crystals destroyed the original cross-linked glass network and led to significantly decreased mechanical strength.

Evidently, the increase in rate of HV in series A was higher than that in series B, as confirmed by the larger slope of linear fitting of the former (Fig. 5). The maximum increase in HV reached 11.5% for series A and 7.3% at most for series B, indicating that the enhancement of microhardness of the SSS ChGs by thermal treatment was composition dependent.

3.4 | Optical property of SSS GCs.

The full-band transmittance spectra of SSS glass and GC samples in the two series are presented in Fig. 6. The transparency range for both SSS ChGs decreased after thermal treatment, which signified the presence of optical scattering loss due to formation of Sb_2Se_3 crystals in the SSS GCs. Considering that optical loss occurred mainly in the short-wavelength region in which the wavelengths were comparable to the size of Sb_2Se_3 crystals, Rayleigh scattering was responsible for the decrease in optical transmittance at the corresponding wavelengths. Therefore, the location of cutoff edge at the long wavelength for the SSS ChGs remained almost unchanged after thermal treatment, and the GC samples treated for <4 h in each series had very similar optical qualities to SSS ChGs.

.

Accepted Article

The inset of Fig. 6 shows that the thermal treatment of SSS ChGs caused an evident shifting of the near-infrared absorption edge to a longer wavelength, i.e., red-shifting, which indicated a decrease in bandgap energy (E_g). Apparently, this decrease was associated with the growth of Sb_2Se_3 crystals in the SSS glass matrix. The formation of such nanoscale semiconductor in a dielectric matrix reportedly causes the appearance of gap states, i.e., an antibonding state of coordination bond, [26] within the band structure. Thus, the growth of Sb_2Se_3 nanocrystals in SSS ChGs allowed the occurrence of electronic transitions from the conduction band to the valance band in the presence of incident photons with low energy, which manifested as the red-shifting of the absorption edge in the short-wavelength region. By defining E_g at incident photon energy in which the linear absorption coefficient (α) was equal to 100 cm^{-1}, [27] the monotone decreasing tendency of E_g with thermal treatment in both series of SSS GCs was achieved (Fig. 7). This finding indicated the availability of thermal treatment to modify the optical property of the SSS ChGs.

4 | DISCUSSION

The experimental results of Swiler et al.[12,13] showed that the hardness of chalcogenide glasses increased linearly with increased MCN in the chalcogen-rich region. However, as shown in Fig. 1, HV increased nonlinearly with increased MCN and stabilized at MCN exceeding 2.4 in the SSS system. A steep increase in HV as MCN approached 2.4 was clearly observed. Phillips–Thorpe's constraint theory[28] states that the transition of covalent glasses from an under-cross-linked floppy network into an over-constrained rigid network occurs at

.

Accepted Article

MCN = 2.4, and that a rapid increase in HV at this threshold MCN is direct evidence of the transition of the SSS glass network from a floppy to a rigid state[29], and this phenomenon is known as rigidity percolation.

To gain insight into the structural property of SSS GCs and discuss the nature of variations in their physical properties resulting from thermal treatment, their Raman spectra were obtained and analyzed. Figs. 8(a) and 8(b) show the normalized Raman spectra measured from the SSS GC samples in series A and B, respectively. A main Raman peak at ~180 cm^{-1} and a secondary peak at ~250 cm^{-1} were present in each spectrum. As noted by the arrows in the spectra, the main peak broadened due to the appearance of a shoulder at 183 cm^{-1}, which belonged to the symmetrical stretching of pyramidal $SbSe_3$. Conversely, the relative intensity of the Raman signal beyond 200 cm^{-1} due to the bending and stretching modes of Se_8 rings weakened after thermal treatment.

By using the Gaussian decomposition method as shown in Figs. 8(c) and 8(d), each Raman spectrum was converted into four overlapped Gaussian peaks at 178, 190, 211, and 252 cm^{-1}, which corresponded to the vibration of tetrahedral $SnSe_4$ and pyramidal $SbSe_3$, as well as the bending and stretching of Se_8 rings, [30, 31] respectively. The normalized integrated area (A_{nor}) of all decomposed peaks was also calculated for quantitative analysis. Fig. 9 illustrates the A_{nor} values of each structural unit as a function of treatment duration. A_{nor} for the symmetrical stretching of pyramidal $SbSe_3$ rapidly increased in both series of SSS GCs.

.

Accepted Article

This finding can be considered as a uniformity process of the Sb-Se heteropolar bonds from the amorphous network, i.e., the crystallization of Sb_2Se_3 phase. The A_{nor} values for both bending and stretching of Se_8 rings slightly decreased with prolonged treatment, indicating that some of the Se-Se homopolar bonds in Se_8 rings broke and were converted into Se-Sb heteropolar bonds after thermal treatment.

Based on the above Raman spectroscopy analysis, the local area involved in the crystallization of the SSS ChG network is depicted in Fig. 10. This result may explain the changes in the SSS glass network after thermal treatment. Regarding the microhardness of the SSS ChGs, as described in Section 3.1, Sb content was found to be the main factor determining the mechanical strength of the glasses. Accordingly, the significant enhancement of the symmetrical stretching of pyramidal [$SbSe_3$] due to the formation of Sb_2Se_3 nanocrystals after thermal treatment can be considered as the reason for the increased HV of the SSS GCs. As shown in Fig. 10, the Sb_2Se_3 crystals had an equilateral-triangle structure in each plane, rendering them tougher and more stable than amorphous $SbSe_3$ pyramids. Thus, the SSS glass network cross-linked by Sb_2Se_3 nanocrystals strengthened, and HV continually increased with prolonged thermal treatment as long as the nanosize of the crystals remained.

.

Accepted Article

5 | CONCLUSIONS

The microhardness of ChGs of the Sn-Sb-Se (SSS) ternary system was investigated. Microhardness rapidly increased as the MCN of the SSS ChGs approached 2.4, signifying the transition of the SSS glass network from under-cross-linked floppy to over-constrained rigid state. This finding well agreed with the prediction of Phillips-Thorpe's constraint theory. Sb content was found to be the main factor determining the microhardness of the SSS ChGs. By thermally treating two selected SSS ChG samples through a one-step process, two series of infrared-transparent SSS GCs were prepared, and the appearance of nanocrystals belonging to Sb_2Se_3 phase in the SSS GCs was confirmed by XRD and SEM analyses. The microhardness of the SSS GCs was found to be improved compared with that of precursor glasses, and this improvement can be attributed to the increased symmetrical stretching of pyramidal $SbSe_3$ resulting from the appearance of Sb_2Se_3 nanocrystals after thermal treatment.

ACKNOWLEDGEMENTS

This work was partially supported by National Natural Science Foundation of China (grant no. 61675106). It was also sponsored by K.C. Wong Magna Fund in Ningbo University.

.

Accepted Article

REFERENCES

1. Zhang X H, Guimond Y, Bellec Y. Production of complex chalcogenide glass optics by molding for thermal imaging. *J Non-Cryst Solids*. 2003; 326[4]: 519-23.

2. Adam J L, Zhang X. *Chalcogenide glasses: preparation, properties and applications*. Sawston, Cambridge: Woodhead Publishing Limited; 2013.

3. Zakery A, Elliott S R. *Optical nonlinearities in chalcogenide glasses and their applications*. Heidelberg : Springer Berlin Heidelberg; 2007.

4. Eggleton B J, Luther-Davies B, Richardson K. Chalcogenide photonics. *Nat Photonics*. 2011; 5[3]: 141-48.

5. Sanghera J S, Aggarwal I D. Active and passive chalcogenide glass optical fibers for IR applications: a review. *J Non-Cryst Solids*. 1999; 256: [16] 6-16.

6. Li L, Lin H, Qiao S, Zou Y, Danto S, Richardson K, et al. Integrated flexible chalcogenide glass photonic devices. *Nat Photonics*. 2015; 8[8]: 643-49.

7. Petersen C R, Møller U, Kubat I, Zhou B, Dupont S, Ramsay J, et al. Mid-infrared supercontinuum covering the 1.4–13.3 μm molecular fingerprint region using ultra-high NA chalcogenide step-index fibre. *Nat Photonics.* 2014; 8[11]: 830-34.

8. Phillips J C. Topology of covalent non-crystalline solids I: short-range order in chalcogenide alloys. *J Non-Cryst Solids.* 1979; 34[2]: 153-81.

.

Accepted Article

9. Chen G, Cheng J. Relationship between the average coordination number and properties of chalconitride glasses. *J Am Ceram Soc.* 2010; 81[6]: 1695-97.

10. Wei W H, Wang R P, Shen X, Fang L, Lutherdavies B. Correlation between structural and physical properties in Ge–Sb–Se glasses. *J Phys Chem C*. 2013;117[32]: 16571–76.

11. Golovchak R, Calvez L, Petracovschi E, Bureau B, Savytskii D, Jain H, et al. Incorporation of Ga into the structure of Ge–Se glasses. *Mate Che. Phys*. 2013;138[2]: 909-16.

12. Swiler D R, Varshneya A K, Callahan R M. Microhardness, surface toughness and average coordination number in chalcogenide glasses. *J Non-Cryst Solids*. 1990;125[3]: 250-57.

13. Sreeram A N, Varshneya A K, Swiler D R. Microhardness and indentation toughness versus average coordination number in isostructural chalcogenide glass systems. *J Non-Cryst Solids*. 1991;130[3]: 225-35.

14. Calvez L, Ma H L, Lucas J, Zhang X H. Glasses and glass-ceramics based on $GeSe_2$–Sb_2Se_3 and halides for far infrared transmission. *J Non-Cryst Solids*. 2008; 354[12]: 1123-27.

15. Guignard M, Nazabal V, Smektala F, Adam J L, Bohnke O, Duverger C, et al. Chalcogenide glasses based on germanium disulfide for second harmonic generation. *Adv Funct Mater*. 2010;17[16]: 3284-94.

16. Zhang X, Hongli M A, Lucas J. A new class of infrared transmitting glass-ceramics based on controlled nucleation and growth of alkali halide in a sulphide based glass matrix. *J Non-Cryst Solids*. 2004; 337[2]: 130-35.

.

Accepted Article

17. Gupta P, Stone A, Woodward N, Dierolf V, Jain H. Laser fabrication of semiconducting ferroelectric single crystal SbSI features on chalcohalide glass. *Opt Mater Express*. 2011; 1[4]: 652-57.

18. Sisken L, Smith C, Buff A, Kang M, Chamma K, Wachtel P, et al. Evidence of spatially selective refractive index modification in $15GeSe_2$-$45As_2Se_3$-40PbSe glass ceramic through correlation of structure and optical property measurements for GRIN applications. *Opt Mater Express*. 2017; 7[9]: 3077-92.

19. Huang Y, Chen F, Qiao B, Dai S, Nie Q, Zhang X, et al. Improved nonlinear optical properties of chalcogenide glasses in Ge-Sn-Se ternary system by thermal treatment. *Opt Mater Express*. 2016; 6[5]: 1644-52.

20. Lin C, Chen F, Zhang Q, Yu Q, Dai S. Performance improvement of transparent germanium–gallium–sulfur glass ceramic by gold doping for third-order optical nonlinearities. *Opt Express*. 2013; 21[21]: 24847-55.

21. Lin C, Calvez L, Ying L, Chen F, Song B A, Shen X, et al. External influence on third-order optical nonlinearity of transparent chalcogenide glass-ceramics. *Appl Phys A*. 2011;104[2]: 615-20.

22. Lin R, Chen F, Zhang X, Huang Y, Song B, Dai S, et al. Mid-infrared optical properties of chalcogenide glasses within tin-antimony-selenium ternary system. *Opt Express*. 2017; 25[21]: 25674-88 .

23. Imran M M A, Lafi O A. Glass transition kinetics and optical band gap in $Se_{85-x}Sb_{15}Sn_x$ (x = 10, 11, 12.5, and 13) chalcogenide glasses. *Mate Chem Phys*. 2011;129[3]: 1201-06.

.

Accepted Article

24. Imran M M A. Thermal characterization of $Se_{85-x}Sb_{15}Sn_x$ ($10 \leq x \leq 13$) chalcogenide glasses. *Physica B*. 2011; 406[22]: 4289-95.

25. Lin C, Rüssel C, Dai S. Chalcogenide glass-ceramics: functional design and crystallization mechanism. *Prog Mater Sci*. 2018; 93: 1-44.

26. Zou L E, He P P, Chen B X, Iso M. Nonlinear optical properties of $As_{20}S_{80}$ system chalcogenide glass using Z-scan and its strip waveguide under bandgap light using the self-phase modulation. *Aip Adv*. 2017; 7[2]: 025003.

27. Fedus K, Boudebs G, Coulombier Q, Troles J, Zhang X H. Nonlinear characterization of GeS_2–Sb_2S_3–CsI glass system. *J Appl Phys*. 2010; 107[2]: 9205.

28. Phillips J C, Thorpe M F. Constraint theory, vector percolation and glass formation. *Solid State Commun.* 1985; 53[8]: 699-702.

29. Kumar P, Thangaraj R. Glassy state and structure of Sn–Sb–Se chalcogenide alloy. *J Non-Cryst Solids*. 2006; 352[21]: 2288-91.

30. Wakkad M M, Shokr E K, Abd E G, A H, Awad M A. Structural and kinetic evaluation of Sn–Sb–Se alloys. *J Phys D-Appl Phys*.2007; 40[23]: 7572-78.

31. Adam A B. Infrared and raman studies on Sn_x–Sb_5–Se_{95-x} chalcogenide glasses. *J King Saud Univ -Sci*. 2009; 21[2]: 93-97.

.

Accepted Article

Figure Captions

Fig. 1. Vickers hardness (HV) as a function of mean coordination number (MCN) for SSS ChGs.

Fig. 2. Vickers hardness (HV) versus Sn content (a) and Sb content (b) for SSS ChGs.

Fig. 3. XRD patterns for SSS GCs in Series A (a) and Series B (b); Identification of the crystal phase formed in GC samples (c).

Fig. 4. SEM images taken from B-SSS-0 (a), B-SSS-2 (b), B-SSS-4 (c), B-SSS-6 (d), B-SSS-8 (e) and B-SSS-10 (f).

Fig. 5. Vickers hardness (HV) as a function of thermal treatment duration for SSS GCs; the red lines are linear fitting.

Fig. 6. Transmittance and absorbance spectra for SSS GCs in Series A (a) and Series B (b); The red arrow in each inset notes red-shifting of the absorption edge.

Fig. 7. Bandgap energy (E_g) as a function of treatment duration for the SSS GC samples.

Fig. 8. Normalized Raman spectra for SSS GCs from Series A (a) and Series B (b); Decomposed Raman spectra of three selected GC samples from Series A (c) and Series B (d).

Fig. 9. Normalized integrate area for all the decomposed Raman peaks as a function of treatment duration.

Fig. 10. Schematic diagram for the local area involved in crystallization process of the SSS ChG network.

.

Accepted Article

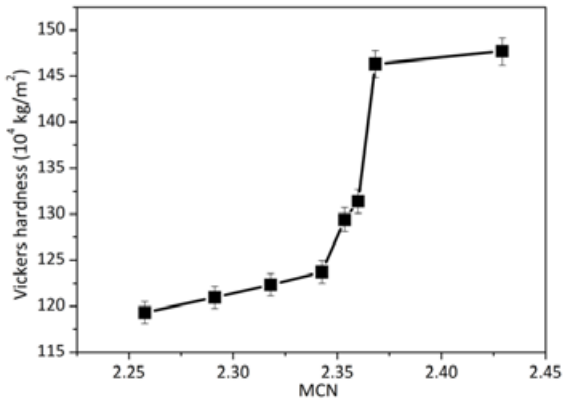
Table

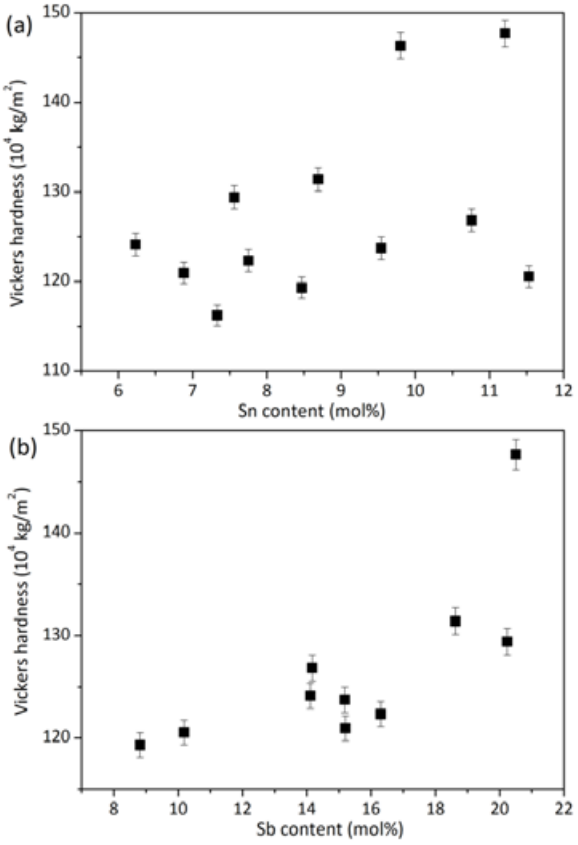
TABLE 1. Glass composition, mean coordination number (MCN) and glass-transition temperature (T_g) of the SSS ChG samples.

Glass composition (at.%)			MCN	T_g (±0.1 K)
Sn	Sb	Se		
8.47	8.82	82.71	2.2576	384.7
6.23	14.11	79.66	2.2657	400.4
7.33	14.38	78.29	2.2904	405.5
6.88	15.2	77.92	2.2912	408.6
7.75	16.3	75.95	2.318	412.8
11.53	10.18	78.29	2.3324	418.5
9.54	15.18	75.28	2.3426	415.3
7.56	20.23	72.21	2.3535	414.5
10.76	14.17	75.07	2.3569	420.5
8.69	18.62	72.69	2.36	418.1
9.8	17.22	72.98	2.3682	430.6
11.21	20.5	68.29	2.4292	429.2

.

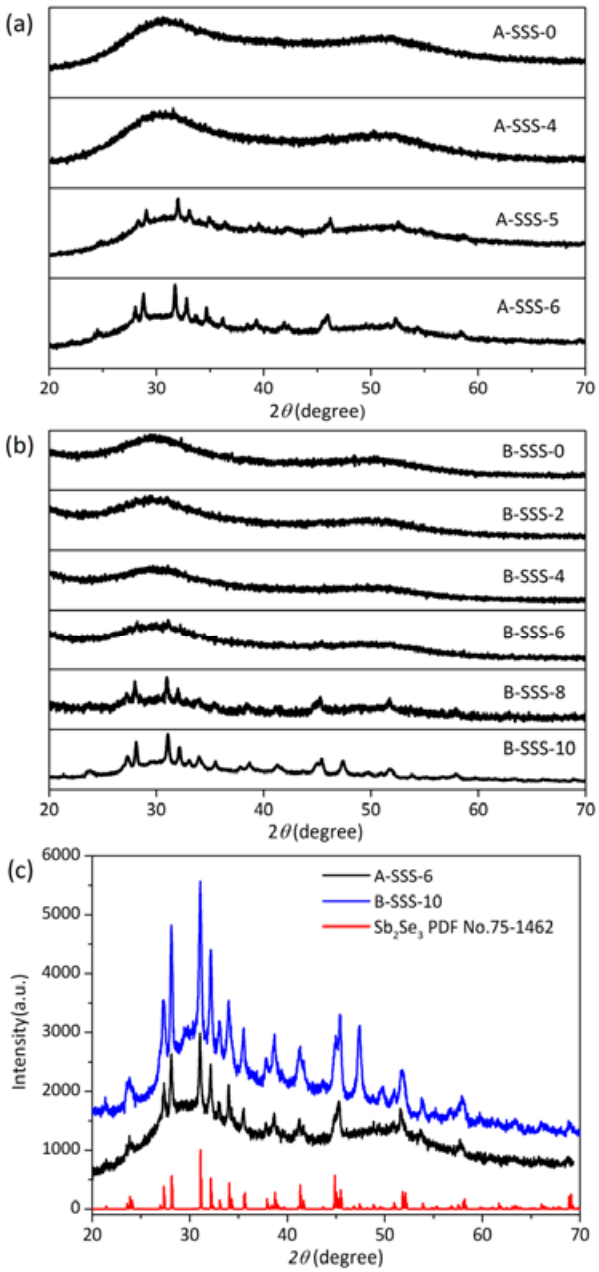
Accepted Article





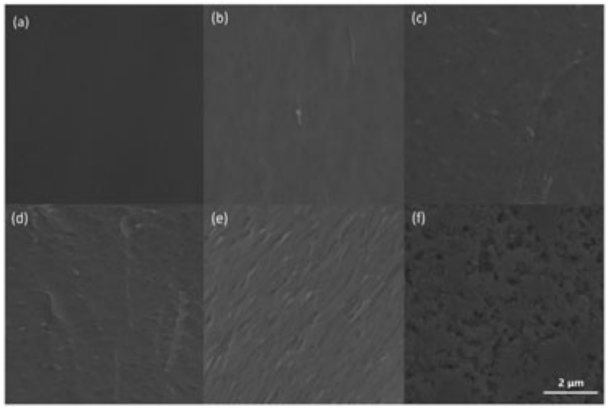
.

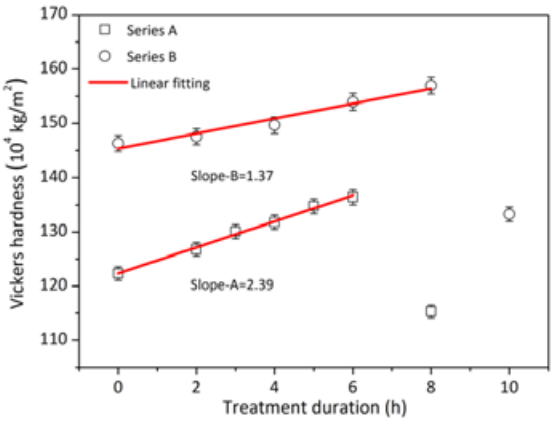
Accepted Article



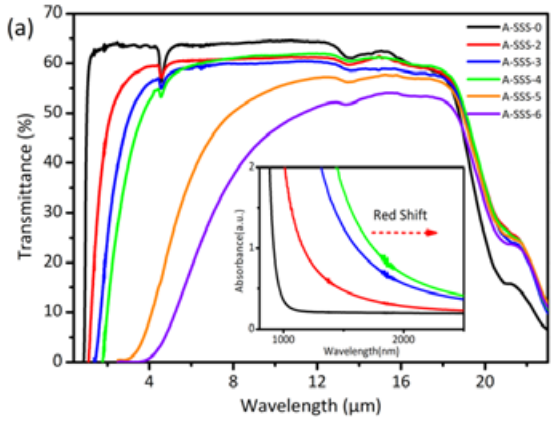
.

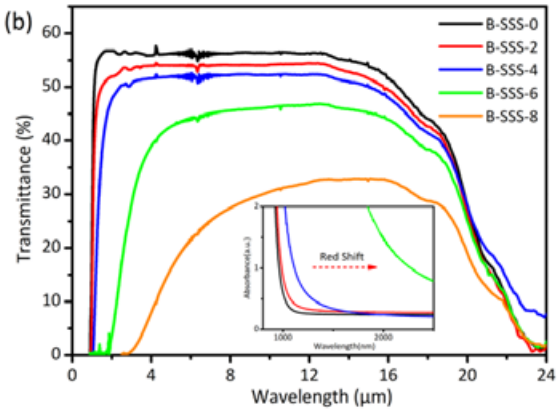
Accepted Article

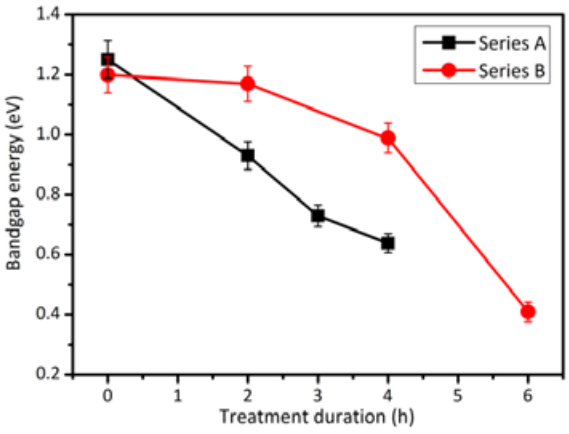




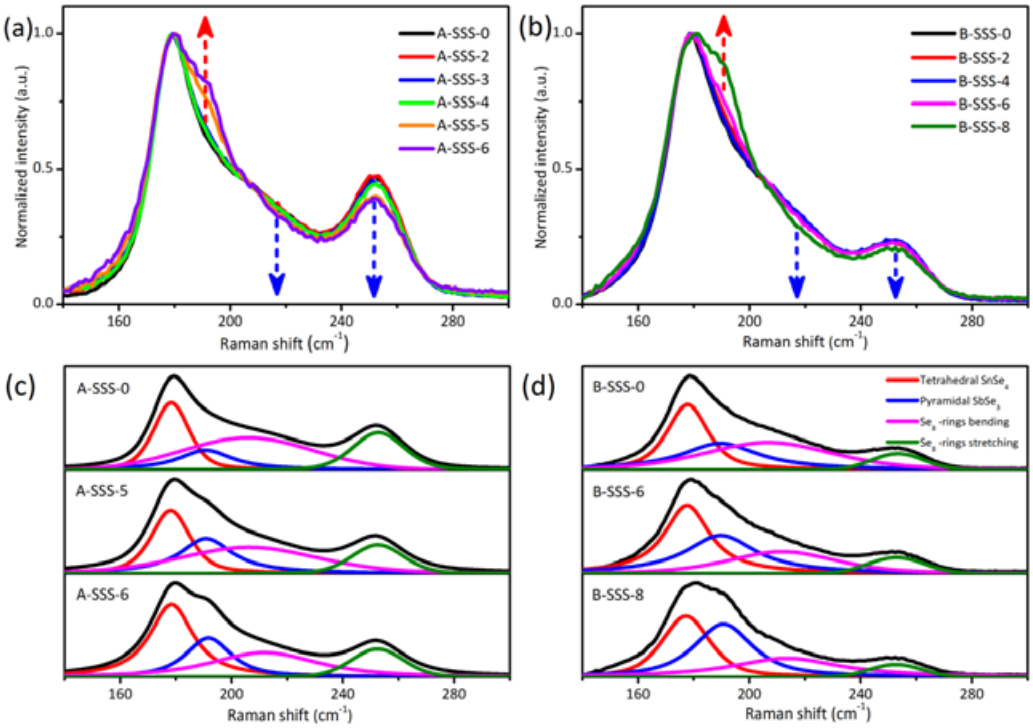
Accepted Article



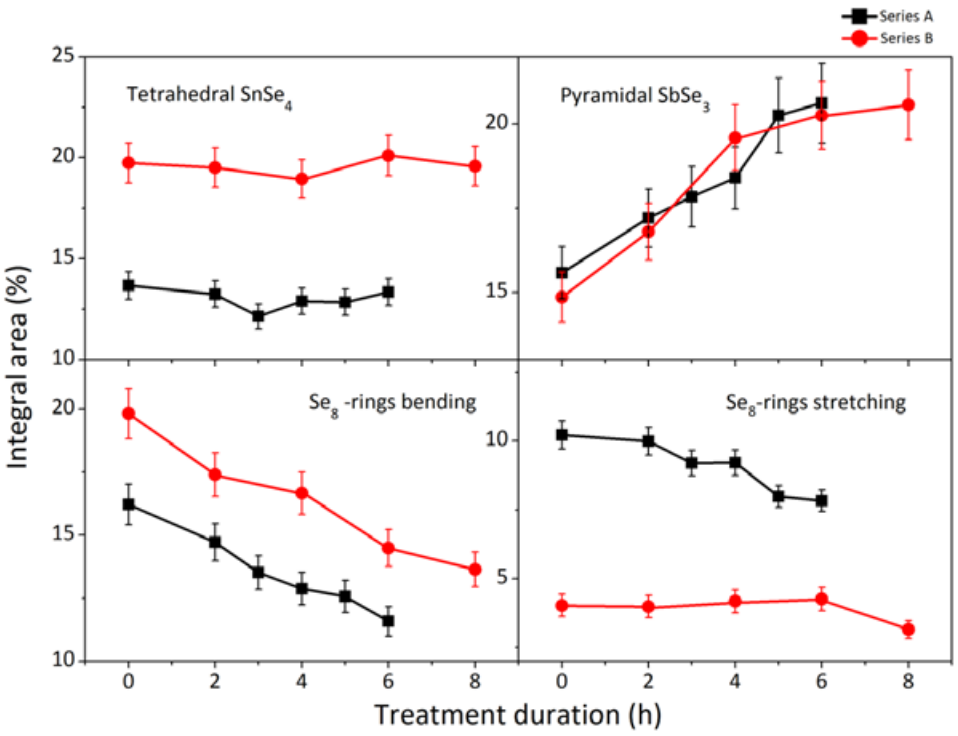


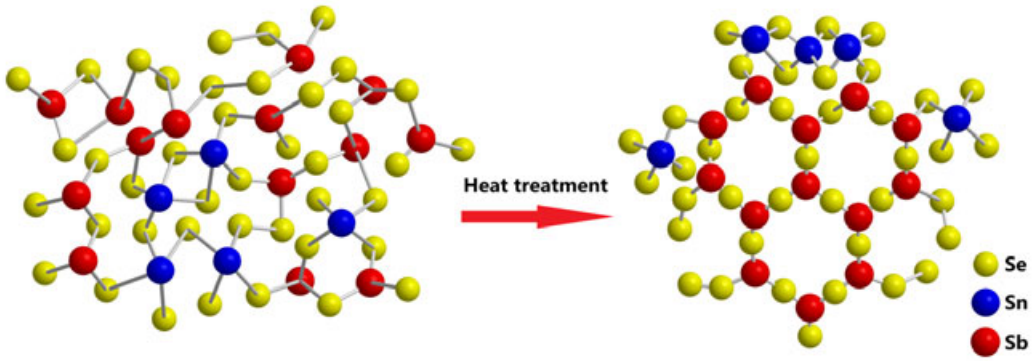


Accepted Article



Accepted Article





.